Journal of Solid State Chemistry **155,** 46–54 (2000)
doi:10.1006/jssc.2000.8890, available online at http://www.idealibrary.com on IDEAL®

Synthesis, Proton Exchange, and Topochemical Dehydration of New Ruddlesden–Popper Tantalates and Titanotantalates[1]

Raymond E. Schaak and Thomas E. Mallouk

Department of Chemistry, Pennsylvania State University, University Park, Pennsylvania 16802

Received May 16, 2000; in revised form July 6, 2000; accepted July 27, 2000

DEDICATED TO PROFESSOR J. M. HONIG

Several new ion-exchangeable Ruddlesden–Popper phases were synthesized and characterized. $K_2CaNaTa_3O_{10}$, which crystallizes in space group *I4/mmm* and has lattice constants of $a = 3.9185(1)$ and $c = 29.519(2)$, is the first all-tantalum(V) analogue of $K_2La_2Ti_3O_{10}$. $K_2Ca_2Ta_2TiO_{10}$ immediately hydrates in air to $K_2Ca_2Ta_2TiO_{10} \cdot 0.8H_2O$, which belongs to space group *P4/mmm* with $a = 3.8903(1)$ and $c = 16.709(1)$. $K_2SrLaTi_2TaO_{10} \cdot 2H_2O$, which contains a large perovskite impurity, also crystallizes in space group *P4/mmm* and has lattice constants of $a = 3.9028(3)$ and $c = 16.896(2)$. All of the phases undergo ion exchange in dilute acid to form the corresponding solid acids. The solid acids topochemically dehydrate around 500°C to form *A*-site defective cubic perovskites. © 2000 Acdemic Press

INTRODUCTION

Ruddlesden–Popper phases (1), $A_2[A'_{n-1}B_nO_{3n+1}]$ (A, A' = alkali, alkaline earth, or rare earth, and B = transition metal), can be described as intergrowths of the perovskite and rocksalt structures. Members of the Ruddlesden–Popper family of layered perovskites possess interesting properties depending on the choice of *A*- and *B*-site cations. For example, Ruddlesden–Popper cuprates such as $La_{2-x}Ba_xCuO_4$ are high-T_c superconductors (2), and manganite phases such as $La_{2-2x}Sr_{1+2x}Mn_2O_7$ exhibit colossal magnetoresistance (3). Many Ruddlesden–Popper and structurally related Dion–Jacobson (4) compounds that contain TiO_6, NbO_6, and TaO_6 octahedra readily exchange their interlayer alkali cations for protons (5–8) or other monovalent (9) and divalent (10) cations, and some of these phases have interesting dielectric (11), catalytic (12), and superconductive (13) properties.

From the point of view of the rational synthesis of new, metastable solids (14), ion-exchangeable Ruddlesden–Popper phases provide convenient precursors that can be chemically modified at low (< 600°C) temperatures and transformed into novel three-dimensional phases. For example, divalent ion exchange of the $n = 3$ phase $K_2Eu_2Ti_3O_{10}$ and subsequent topochemical reduction forms the *A*-site ordered nondefective perovskites $AEu_2Ti_3O_9$ (A = Ca, Sr) (15). Novel *A*-site defective cubic perovskites such as $La_{2/3}TiO_3$ (7) and $SrTa_{2-x}Nb_xO_6$ (16) and defective Ruddlesden–Popper phases such as $Ln_2Ti_2O_7$ (17) can be synthesized by topochemically dehydrating the appropriate Ruddlesden–Popper acids. Interesting Aurivillius phases (18) and perovskite–copper halide intergrowths (19) can also be topochemically synthesized from Ruddlesden–Popper and Dion–Jacobson phases.

One of the challenges limiting the rational design of new solids from lamellar precursors is the availability of the appropriate Ruddlesden–Popper phases. Only a small number of ion-exchangeable Ruddlesden–Popper phases have been reported, and their syntheses are often hindered by decomposition to more stable ABO_3 phases or by competition between multiple lamellar phases that are thermodynamically stable. In this paper, we present the direct synthesis and characterization of several new $n = 3$ members of the Ruddlesden–Popper series. These new tantalum-rich phases readily exchange their interlayer alkali cations for protons, and the resulting solid acids can be topochemically dehydrated to form new *A*-site defective cubic perovskites.

EXPERIMENTAL

Synthesis

$K_2CaNaTa_3O_{10}$ was initially synthesized by the solid-state reaction of K_2CO_3 (Aldrich, 99.99%), $CaCO_3$ (Aldrich, 99.995%), Na_2CO_3 (Aldrich, 99.95%), and Ta_2O_5 (Aldrich, 99.99%) at 1300°C for 12 h. Higher-purity $K_2CaNaTa_3O_{10}$ was synthesized using a procedure similar to that of Kodenkandath and Wiley (20), substituting KOH (Aldrich, 85%) for K_2CO_3 and reacting the intimately mixed solids for 12 h at 1050°C, followed by 6 h at 1100°C.

[1] This paper is dedicated to Professor J. M. Honig, in thanks for his friendship, his scientific accomplishments, and his many years of service to the community of solid state chemistry.

0022-4596/00 $35.00

$K_2Ca_2Ta_2TiO_{10}$ was synthesized by heating KOH, $CaCO_3$, Ta_2O_5, and TiO_2 (Aldrich, 99.9%) to 1300°C for 60 min. $K_2Sr_2Ta_2TiO_{10}$ was synthesized by heating K_2CO_3, $SrCO_3$ (Alfa–Aesar, 99.99%), Ta_2O_5, and TiO_2 to 1200°C for 12 h. $K_2SrLaTi_2TaO_{10}$ was synthesized by heating K_2CO_3, $SrCO_3$, La_2O_3 (Aldrich, 99.99%), TiO_2, and Ta_2O_5 at 1300°C for 12 h. $K_2CaLaTi_2TaO_{10}$ was synthesized by reacting KOH, $CaCO_3$, La_2O_3, TiO_2, and Ta_2O_5 at 1300°C for 60 min. In all cases, a 40% excess of alkali carbonate and alkali hydroxide was used to account for loss due to volatilization and for water content in the hydroxide.

All of the layered solids were proton-exchanged in 0.1 M HNO_3 for 5 days at room temperature. The acid was renewed daily to ensure complete exchange. In some cases, only one or two days were necessary for complete exchange to occur. The solid acids were topochemically dehydrated by heating them to 500°C for 4 h.

Instrumentation

X-ray diffraction (XRD) patterns were obtained on a Philips X-Pert MPD diffractometer using monochromatized Cu$K\alpha$ ($\lambda = 1.5418$ Å) radiation. Diffraction patterns from powdered samples held on a quartz zero background plate were obtained in 2θ geometry. Lattice parameters and atomic positions were determined by the Rietveld method using the GSAS structure refinement package (21).

Energy-dispersive X-ray emission analysis (EDAX) was performed using a JEOL-JSM 5400 scanning electron microscope at 30 kV accelerating voltage. EDAX data was obtained at the Electron Microscope Facility for the Life Sciences in the Biotechnology Institute at the Pennsylvania State University. Typically, data from several acquisitions were averaged to obtain the reported results.

Thermal gravimetric analysis (TGA) was obtained using a TA Instruments TGA 2050. Data were collected in air from 25 to 1000°C at a heating rate of 10°C/min.

RESULTS AND DISCUSSION

Synthesis of New Ruddlesden–Popper Phases

Synthesizing new ion-exchangeable Ruddlesden–Popper phases is often problematic, since decomposition and thermodynamic instabilities limit the compositions that can form the layered perovskite structure. While phases such as $K_2La_2Ti_3O_{10}$ are easily synthesized by reacting the constituent oxides and carbonates at 1100°C for one day (7), synthesizing other phases requires some modified approaches. For example, the $n = 2$ phase $K_2SrTa_2O_7$ has an ABO_3 impurity phase (16), which can be minimized using KOH as the alkali source (20). The $n = 1$ phase $NaLaTiO_4$ is unstable relative to the $n = 3$ phase $Na_2La_2Ti_3O_{10}$, so a short 30-min reaction time isolates the desired kinetic phase (22). In contrast, the thermodynamic $n = 2$ phase $Li_2SrNb_2O_7$ requires several days of heating to produce a phase-pure material (23).

In the case of the $n = 3$ Ruddlesden–Popper phases, few examples other than the well-studied $K_2Ln_2Ti_3O_{10}$ series exist (7). Substitution of Nb^{5+} for Ti^{4+} has allowed for the synthesis of $K_2Ca_2Nb_2TiO_{10}$, which contains a large amount of perovskite impurity (8). Also, the mixed-valent tantalates $A_2Ca_2Ta_3O_{10}$ (A = Na, Li) have been topochemically synthesized from phase-pure Dion–Jacobson compounds by using reductive intercalation (24). To our knowledge, no examples of $n = 3$ Ruddlesden–Popper tantalates and titanotantalates that contain only Ta^{5+} (and not Nb^{5+}) have been reported to date.

By combining several synthetic approaches, we were able to synthesize several new $n = 3$ Ruddlesden–Popper phases. $K_2CaNaTa_3O_{10}$, the first all-tantalum(V) analogue of $K_2La_2Ti_3O_{10}$, can be synthesized using K_2CO_3 at 1300°C, but the high reaction temperature guarantees that decomposition will occur. Following the approach of Kodenkandath and Wiley (20), we used the lower-melting KOH instead of K_2CO_3 to lower the reaction temperature (in this case, to 1100°C) and minimize the decomposition. The next member of the titanotantalate series, $K_2Ca_2Ta_2TiO_{10}\cdot 0.8H_2O$, was synthesized as a phase-pure material by using KOH and limiting the reaction time to 60 min. The titanotantalate $K_2SrLaTi_2TaO_{10}\cdot 2H_2O$ could only be synthesized at 1300°C using K_2CO_3, so a perovskite impurity phase was unavoidable.

Structure of $K_2CaNaTa_3O_{10}$

$K_2CaNaTa_3O_{10}$ crystallizes in space group $I4/mmm$ and is isostructural with its titanium analogue, $K_2La_2Ti_3O_{10}$ (25). As indicated in Table 1, the a axis lattice parameter of

TABLE 1
Lattice Parameters[a]

Compound	a, Å	c, Å
$K_2CaNaTa_3O_{10}$	3.9185(1)	29.519(2)
$K_2Ca_2Ta_2TiO_{10}\cdot 0.8H_2O$	3.8903(1)	16.709(1)
$K_2Sr_2Ta_2TiO_{10}\cdot xH_2O$	3.9124(4)	16.906(2)
$K_2SrLaTi_2TaO_{10}\cdot 2H_2O$	3.9028(3)	16.896(2)
$K_2CaLaTi_2TaO_{10}\cdot xH_2O$	3.8897(3)	16.799(5)
$H_2CaNaTa_3O_{10}$	3.8851(7)	26.98(1)
$H_2Ca_2Ta_2TiO_{10}$	3.8843(5)	26.66(2)
$H_2Sr_2Ta_2TiO_{10}$	3.9101(3)	27.646(2)
$H_2SrLaTi_2TaO_{10}\cdot xH_2O$	3.898(2)	31.20(2)
$H_2CaLaTi_2TaO_{10}\cdot xH_2O$	3.895(2)	31.97(1)
$CaNaTa_3O_9$	3.890(1)	
$Ca_2Ta_2TiO_9$	3.867(1)	3.950(2)
$Sr_2Ta_2TiO_9$	3.9137(7)	
$SrLaTi_2TaO_9$	3.911(1)	
$CaLaTi_2TaO_9$	3.914(2)	

[a] Standard deviations are given in parentheses.

$K_2CaNaTa_3O_{10}$ is 3.9185 Å, which is significantly larger than that of $K_2La_2Ti_3O_{10}$ (3.8769 Å) and reflects the larger size of the Ta^{5+} cation. The *c* axis lattice parameter of $K_2CaNaTa_3O_{10}$ (29.519 Å) is contracted slightly relative to that of $K_2La_2Ti_3O_{10}$ (29.824 Å). The difference may reflect the electrostatic repulsion of the interlayer potassium and the trivalent lanthanum ions in the perovskite block of $K_2La_2Ti_3O_{10}$; by comparison, there is lower *A*-site charge from Ca^{2+}/Na^{+} in $K_2CaNaTa_3O_{10}$.

EDAX indicates that the stoichiometric ratio of K:Ca:Na:Ta is 2.0:0.85:0.89:3.4, which is consistent with the formula $K_2CaNaTa_3O_{10}$ along with a minor potassium tantalate impurity. EDAX analysis of the proton-exchanged form $H_2CaNaTa_3O_{10}$ indicates that most (approx. 90%) of the potassium is removed during the ion exchange, which is consistent with the structural model that places the sodium in the *A* site of the perovskite block rather than mixed with the potassium in the interlayer gallery.

Rietveld structural analysis, shown in Fig. 1, confirms that $K_2CaNaTa_3O_{10}$ is an $n = 3$ member of the Ruddlesden–Popper series. The fractional coordinates, site occupancies, and thermal parameters obtained from the refinement are given in Table 2. The refinement converged reasonably well to give $R_f^2 = 8.52\%$, $R_{wp} = 12.98\%$, $R_p = 9.70\%$, and $\chi^2 = 2.36$. The reliability factors are somewhat high due to the presence of a small perovskite impurity. The impurity peaks, which are characterized by low-intensity broadened bands in the X-ray diffraction pattern, are evident in the difference curve of the Rietveld refinement. No low-angle reflections consistent with lower-order $n = 1$ or $n = 2$ layered perovskite phases were observed, so the impurity is likely an ABO_3 perovskite phase. High-resolution electron microscopy studies may prove useful in identifying the impurity phase(s). Attempts to include the impurity phase in the refinement model gave only slight improvements in the fit.

The structure of $K_2CaNaTa_3O_{10}$, shown in Fig. 2a, consists of $CaNaTa_3O_{10}^{2-}$ triple-layer perovskite slabs interleaved with K^+ in a rocksalt-type layer. The perovskite layers are staggered along the (110) direction. The Ca and Na cations are statistically distributed among the perovskite *A* sites, while Ta occupies the *B* sites. As in most layered perovskites, the Ta atoms closest to the interlayer gallery are displaced out of the symmetric octahedron, although the distortion is not as significant as in $K_2Ca_2Ta_2TiO_{10}\cdot 0.8H_2O$ or $K_2La_2Ti_3O_{10}\cdot 2H_2O$. Typically, divalent and trivalent cations occupy the perovskite *A* sites, and the outer *B*-site cations (Ta^{5+}, Ti^{4+}) move away from the *A*-site cations toward the monovalent interlayer cations, which have less positive charge (26). Since monovalent Na^+ occupies half of the *A* sites in the perovskite block of $K_2CaNaTa_3O_{10}$, there is less electrostatic repulsion to force the *B*-site cation toward the interlayer.

There are three distinct Ta–O bond lengths in $K_2CaNaTa_3O_{10}$, although they span a narrow range. The outer octahedra, which have the Ta shifted slightly toward the interlayer, have a Ta(2)–O(4) bond length of 1.848 Å, while the inner Ta(2)–O(2) bond is 1.963 Å. The inner Ta(1)-O(2) bonds are slightly longer at 2.096 Å. All of these bond lengths are consistent with those found in other Ruddlesden–Popper tantalates (27).

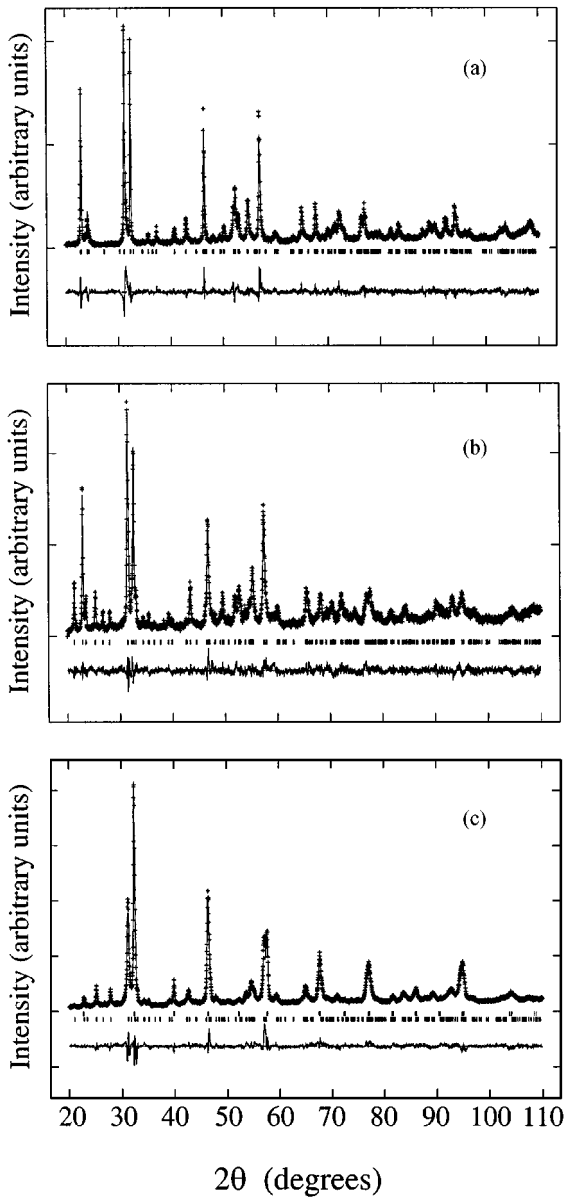

FIG. 1. Rietveld refinements of (a) $K_2CaNaTa_3O_{10}$, (b) $K_2Ca_2Ta_2TiO_{10}\cdot 0.8H_2O$, and (c) $K_2SrLaTi_2TaO_{10}\cdot 2H_2O$, showing the calculated (top, solid line) and observed (top, crosses) XRD patterns. The difference curves (bottom, solid line) indicate the agreement between the observed and calculated patterns. Bragg reflections are marked below the peaks.

Like its titanium analogue, $K_2CaNaTa_3O_{10}$ hydrates over time under ambient conditions. While $K_2La_2Ti_3O_{10}$ forms a crystalline dihydrate (25), $K_2CaNaTa_3O_{10}$ appears to have several levels of hydration. When exposed to a fully

TABLE 2
Crystallographic Data for $K_2CaNaTa_3O_{10}$, $K_2Ca_2Ta_2TiO_{10}\cdot 0.8H_2O$, and $K_2SrLaTi_2TaO_{10}\cdot 2H_2O$

Compound	Atom	Site occupancy	x	y	z	100 U_{iso} (Å^2)	Wyckoff symmetry
$K_2CaNaTa_3O_{10}$[a]	K	1.09(2)	0	0	0.2904(4)	0.8(2)	4e
	Ca	0.55(1)	0	0	0.4229(4)	0.3(2)	4e
	Na	0.56(3)	0	0	0.4229(4)	0.3(2)	4e
	Ta(1)	1.01(1)	0	0	0	0.65(10)	2a
	Ta(2)	0.96(1)	0	0	0.1375(1)	0.77(6)	4e
	O(1)	0.94(6)	0	0.5	0	0.9(8)	4c
	O(2)	0.96(4)	0	0	0.071(2)	3.0(9)	4e
	O(3)	0.94(5)	0	0.5	0.134(1)	2.9(7)	8g
	O(4)	0.99(6)	0	0	0.2001(9)	1.4(9)	4e
$K_2Ca_2Ta_2TiO_{10}\cdot 0.8H_2O$[b]	K	0.94(1)	0.5	0.5	0.381(1)	3.7(3)	2h
	Ca	1.04(1)	0.5	0.5	0.1190(7)	1.8(2)	2h
	Ta(1)	0.653(6)	0	0	0	0.09(8)	1a
	Ta(2)	0.675(6)	0	0	0.2444(2)	0.19(6)	2g
	Ti(1)	0.29(2)	0	0	0	0.09(8)	1a
	Ti(2)	0.35(2)	0	0	0.2444(2)	0.19(6)	2g
	O(1)	0.99(5)	0	0.5	0	2.5(8)	2f
	O(2)	0.95(3)	0	0	0.106(2)	3.2(9)	2g
	O(3)	1.00(3)	0	0.5	0.232(2)	2.4(6)	4i
	O(4)	0.96(3)	0	0	0.365(2)	5.5(9)	2g
	O(5)	0.41(2)	0.21(1)	0	0.5	6(2)	4m
$K_2SrLaTi_2TaO_{10}\cdot 2H_2O$[c]	K	1.03(3)	0.5	0.5	0.380(1)	0.9(5)	2h
	Sr	0.40(1)	0.5	0.5	0.1198(7)	1.2(2)	2h
	La	0.466(9)	0.5	0.5	0.1198(7)	1.2(2)	2h
	Ti(1)	0.54(3)	0	0	0	1.2(3)	1a
	Ti(2)	0.78(2)	0	0	0.2485(4)	0.1(1)	2g
	Ta(1)	0.313(8)	0	0	0	1.2(3)	1a
	Ta(2)	0.358(6)	0	0	0.2485(4)	0.1(1)	2g
	O(1)	1.15(7)	0	0.5	0	3.1(9)	2f
	O(2)	0.95(5)	0	0	0.108(2)	1.4(9)	2g
	O(3)	1.04(4)	0	0.5	0.222(2)	1.0(7)	4I
	O(4)	0.91(5)	0	0	0.356(3)	4(2)	2g

[a] *I4/mmm* (No. 139), $a = 3.9185(1)$ Å, $c = 29.519(2)$ Å.
[b] *P4/mmm* (No. 123), $a = 3.8903(1)$ Å, $c = 16.709(1)$ Å.
[c] *P4/mmm* (No. 123), $a = 3.9028(3)$ Å, $c = 16.896(2)$ Å.

hydrated atmosphere for three days, $K_2CaNaTa_3O_{10}$ intercalates approximately 10 water molecules per formula unit. No plateau of water intake was observed. The resulting solid is poorly crystalline, as evidenced by significant line broadening of the (00*l*) peaks.

Structure of $K_2Ca_2Ta_2TiO_{10}\cdot 0.8H_2O$

Anhydrous $K_2Ca_2Ta_2TiO_{10}$ hydrates immediately upon exposure to air. TGA analysis indicates that there are 0.8 waters of hydration per formula unit. While most hydrated layered perovskites intercalate two water molecules per unit cell, other examples such as $NaEuTiO_4\cdot 0.5H_2O$ (28), $NaEuTiO_4\cdot 0.8H_2O$ (28), and $NaLaNb_2O_7\cdot 1.6H_2O$ (29) have been reported. $K_2Ca_2Ta_2TiO_{10}\cdot 0.8H_2O$ crystallizes in space group *P4/mmm* and is isostructural with $K_2La_2Ti_3O_{10}\cdot 2H_2O$ (25). EDAX analysis confirms that the elemental ratios of K:Ca:Ta:Ti are 2.0:2.4:2.0:1.2, which matches the predicted stoichiometry and a small calcium titanate impurity.

The lattice parameters of $K_2Ca_2Ta_2TiO_{10}\cdot 0.8H_2O$ are $a = 3.8903$ Å and $c = 16.709$ Å, which are slightly smaller than those of $K_2CaNaTa_3O_{10}$, reflecting the smaller size of the Ti^{4+} cation that occupies 1/3 of the perovskite *B* sites. The smaller lattice parameters could also indicate a slight contraction of the unit cell due to the higher *A*-site charge density in $K_2Ca_2Ta_2TiO_{10}\cdot 0.8H_2O$ relative to $K_2CaNaTa_3O_{10}$. As expected, the *a* axis lattice parameter is slightly larger than that of $K_2La_2Ti_3O_{10}\cdot 2H_2O$ ($a = 3.8585$ Å, $c = 16.814$ Å), whereas the *c* axis parameter is slightly contracted.

Rietveld structure refinement, shown in Fig. 1b, confirms that $K_2Ca_2Ta_2TiO_{10}\cdot 0.8H_2O$ is isostructural with $K_2La_2Ti_3O_{10}\cdot 2H_2O$ (25). The refinement in space group

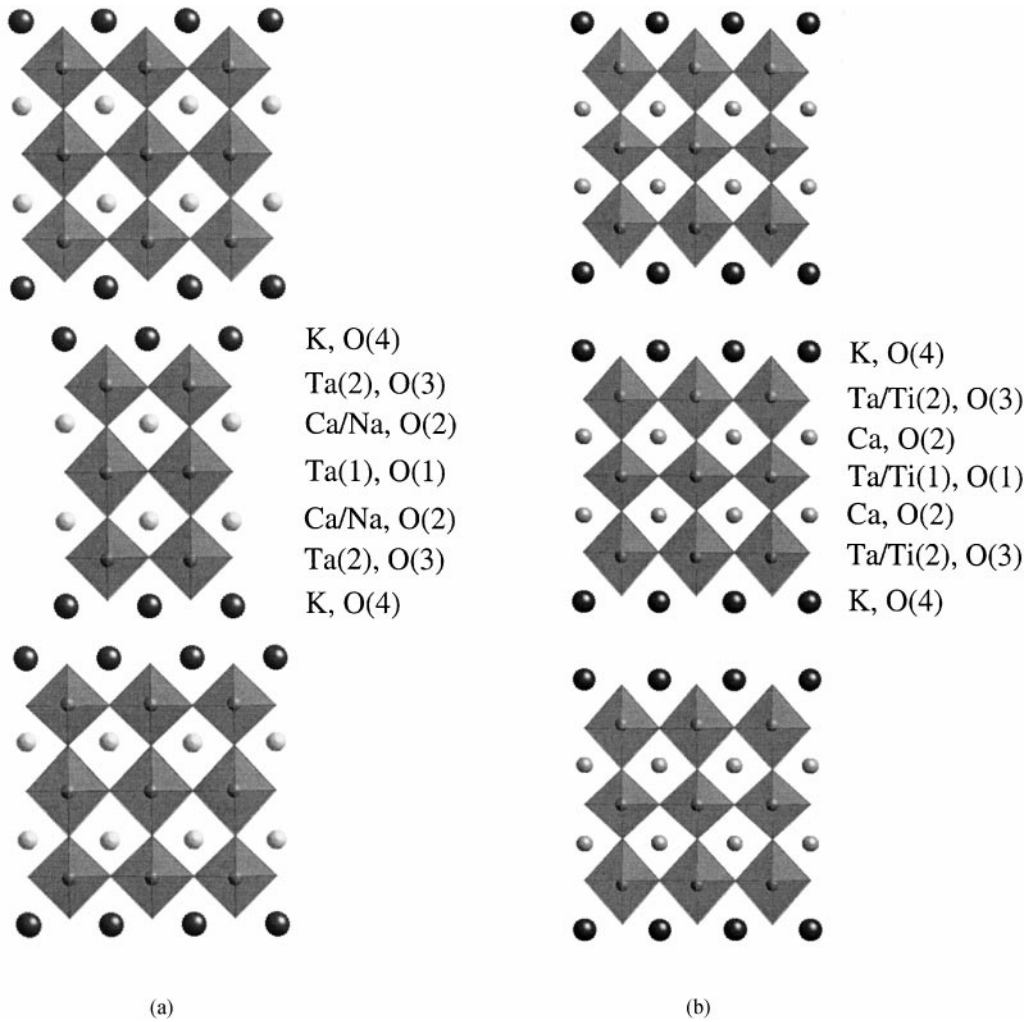

FIG. 2. Crystal structures of (a) $K_2CaNaTa_3O_{10}$ and (b) $K_2Ca_2Ta_2\ TiO_{10}\cdot 0.8H_2O$, viewed along the *a* axis. Atom numbering is the same as in Table 2. Note the more pronounced distortions of the MO_6 octahedra in $K_2Ca_2Ta_2TiO_{10}\cdot 0.8H_2O$.

*P*4/*mmm* quickly converged, yielding $R_f^2 = 9.73\%$, $R_{wp} = 12.65\%$, $R_p = 9.95\%$, and $\chi^2 = 1.96$. The site occupancies did not deviate significantly from those expected from stoichiometry. The atomic positions and thermal parameters changed slightly, reflecting the structural distortions that are discussed below. The fractional coordinates, site occupancies, and thermal parameters are given in Table 2. Attempts to refine the structure in lower symmetry space groups were unsuccessful.

Unlike $K_2CaNaTa_3O_{10}$, which forms a poorly crystalline hydrate, $K_2Ca_2Ta_2TiO_{10}\cdot 0.8H_2O$ remains highly crystalline upon intercalation of water. The oxygen atoms of the interlayer water molecules were included in the refinement, placed on the 4m site as in $K_2La_2Ti_3O_{10}\cdot 2H_2O$ (25). Refinements that did not include the oxygen atoms of the interlayer water yielded slightly higher R_f^2 values. A small perovskite impurity phase that is most likely $CaTiO_3$, based on the higher elemental ratios of Ca and Ti relative to Na and Ta, was observed but not included in the final refinement.

$K_2Ca_2Ta_2TiO_{10}\cdot 0.8H_2O$ (Fig. 2b) consists of $Ca_2Ta_2TiO_{10}^{2-}$ slabs that are eclipsed along the (110) direction. The eclipsed configuration has been noted in other hydrated layered perovskites (20, 28), and most likely allows better coordination of the interlayer potassium with the intercalated water.

The TaO_6/TiO_6 octahedra in $K_2Ca_2Ta_2TiO_{10}\cdot 0.8H_2O$ are axially distorted relative to the bonds in $K_2La_2Ti_3O_{10}$. In the triple-layer perovskite slab, the Ta/Ti cations on the 2g site are displaced toward the interlayer relative to the plane of the equatorial oxygen atoms. This distortion fixes the Ta(2)–O(4) bond at 2.014 Å and the Ta(2)–O(2) bond at 2.305 Å. These values are consistent with the weakest bonds in other hydrated Ruddlesden–Popper phases such as

$K_2SrTa_2O_7 \cdot 2H_2O$ (20) and $NaEuTiO_4 \cdot 0.8H_2O$ (28). The Ta(1)–O(2) bond is relatively short at 1.777 Å, but this bond length is not unreasonable for a 6-coordinate Ta–O bond along the interlayer gallery of a layered perovskite (27).

The Ti and Ta ions are statistically distributed among the *B* sites of the perovskite block. The possibility that Ti occupies the middle row of the triple perovskite block and that Ta occupies the sites adjacent to the interlayer was explored, but the structural model based on *B*-site ordering was not consistent with the powder diffraction data. Likewise, refinement of the site occupancies for the Ti and Ta at both sites did not diverge significantly from the stoichiometric ratios 1/3 and 2/3, respectively. The high thermal parameters for the interlayer potassium and O(4) oxygen atom indicate that there may be some disorder and distortion along the interlayer gallery, from the waters of hydration that may be partially amorphous.

$K_2Sr_2Ta_2TiO_{10} \cdot xH_2O$ could also be synthesized, but only using K_2CO_3 and heating the reaction mixture to 1200°C for several hours. As a result, a large amount of perovskite impurity was present. As shown in Table 1, $K_2Sr_2Ta_2TiO_{10} \cdot xH_2O$ had slightly larger lattice parameters than $K_2Ca_2Ta_2TiO_{10} \cdot 0.8H_2O$, reflecting the larger Sr^{2+} cation relative to Ca^{2+}.

Structure of $K_2SrLaTi_2TaO_{10} \cdot 2H_2O$

Like $K_2Ca_2Ta_2TiO_{10}$, $K_2SrLaTi_2TaO_{10}$ hydrates immediately upon exposure to air, so its anhydrous form could not be isolated. TGA analysis shows two waters of hydration per formula unit (30). High-temperature XRD shows that the anhydrous form has *I*4/*mmm* symmetry as in $K_2La_2Ti_3O_{10}$, but the hydrate adopts the eclipsed *P*4/*mmm* symmetry. The lattice parameters of $K_2SrLaTi_2TaO_{10} \cdot 2H_2O$ are slightly larger than those of $K_2Ca_2Ta_2TiO_{10} \cdot 0.8H_2O$, reflecting the larger Sr^{2+} and La^{3+} cations. EDAX analysis indicates that the stoichiometric ratios of K:Sr:La:Ti:Ta are 3.1:0.68:0.78:1.8:2.0, which is consistent with the stoichiometry of $K_2SrLaTi_2TaO_{10}$ and a large amount of potassium tantalate impurity.

Rietveld structure refinement showed that $K_2SrLaTi_2TaO_{10} \cdot 2H_2O$ is isostructural with $K_2Ca_2Ta_2TiO_{10} \cdot 0.8H_2O$. The structure refinement in space group *P*4/*mmm*, shown in Fig. 1c, converged to $R_f^2 = 10.91\%$, $R_{wp} = 10.39\%$, $R_p = 7.90\%$, and $\chi^2 = 3.02$, which included a second perovskite impurity phase. The atomic positions and thermal parameters, which are included in Table 2, are similar to those of $K_2Ca_2Ta_2TiO_{10} \cdot 0.8H_2O$ (Fig. 2b), indicating that the same structural distortions of the TaO_6/TiO_6 octahedra occur in $K_2SrLaTi_2TaO_{10} \cdot 2H_2O$. The Ta and Ti cations are statistically distributed among the perovskite *B* sites, and Sr and La are statistically distributed among the *A* sites. Based on the refined site occupancies, Ti seems to have a slight preference for the 2g site relative to the 1a site. *B*-site cation ordering was considered, but the structural models were inconsistent with the powder diffraction data.

$K_2CaLaTi_2TaO_{10} \cdot xH_2O$ could also be synthesized, but only using KOH and limiting the synthesis time to 60 min at 1300°C. A major ABO_3 impurity could not be avoided, even with careful synthesis considerations. $K_2CaLaTi_2TaO_{10} \cdot xH_2O$ has slightly smaller lattice parameters than $K_2SrLaTi_2TaO_{10} \cdot 2H_2O$, which is consistent with the smaller size of the Ca^{2+} cation relative to Sr^{2+}.

Proton Exchange of Ruddlesden-Popper Phases

All of the Ruddlesden–Popper tantalates and titanotantalates exchange their interlayer potassium cations for protons in dilute acid, resulting in solid layered acids. Most ion exchanges in Ruddlesden–Popper and Dion–Jacobson phases are nearly stoichiometric, but it is not uncommon to retain a few percent of residual alkali after the ion exchange is complete, presumably due to the substitution of alkali into the *A* sites of the perovskite block (11). For the tantalates and titanotantalates presented in this study, the percent exchange was judged to be as complete as exchanges in other Ruddlesden–Popper systems. EDAX confirmed that much of the potassium was gone after several days of proton exchange, but residual potassium was observed. Quantitation is difficult, since in many cases potassium tantalate or other alkali impurities that remain unchanged throughout the acid exchange add to the potassium signal during EDAX analysis.

$H_2CaNaTa_3O_{10}$, the powder pattern of which is shown in Fig. 3a, retains the *I*4/*mmm* symmetry of its alkali form. The lattice parameter for the *a* axis decreases slightly to 3.8851 Å, while the *c* axis contracts substantially from 29.519 Å in $K_2CaNaTa_3O_{10}$ to 26.98 Å in $H_2CaNaTa_3O_{10}$. As shown in Fig. 3b, $H_2Ca_2Ta_2TiO_{10}$, is isostructural with $H_2CaNaTa_3O_{10}$, indicating that the proton-exchanged form does not hydrate like the alkali $K_2Ca_2Ta_2TiO_{10} \cdot 0.8H_2O$ form. As expected, the lattice parameter in the *a* direction decreases slightly to 3.8843 Å, and the *c* axis contracts to 26.66 Å. The presence of broad peaks in the diffraction patterns of $H_2CaNaTa_3O_{10}$ and $H_2Ca_2Ta_2TiO_{10}$ indicates the possibility that a small amount of acid hydrolysis occurred during the proton exchange.

$H_2SrLaTi_2TaO_{10}$ and $H_2CaLaTi_2TaO_{10}$ exist in both anhydrous and hydrated forms. The hydrated forms, shown in Fig. 3c, appear to adopt *I*4/*mmm* symmetry rather than the eclipsed *P*4/*mmm* symmetry of the hydrated alkali forms. Drying the solid acids at 100°C yields the anhydrous forms (which are also *I*4/*mmm*), but the anhydrous forms cannot be isolated without the onset of irreversible phase transitions since the solids begin to topochemically dehydrate around 100°C. In Figs. 3a–3c, peaks such as those near 40° (which correspond to the cubic perovskite phase

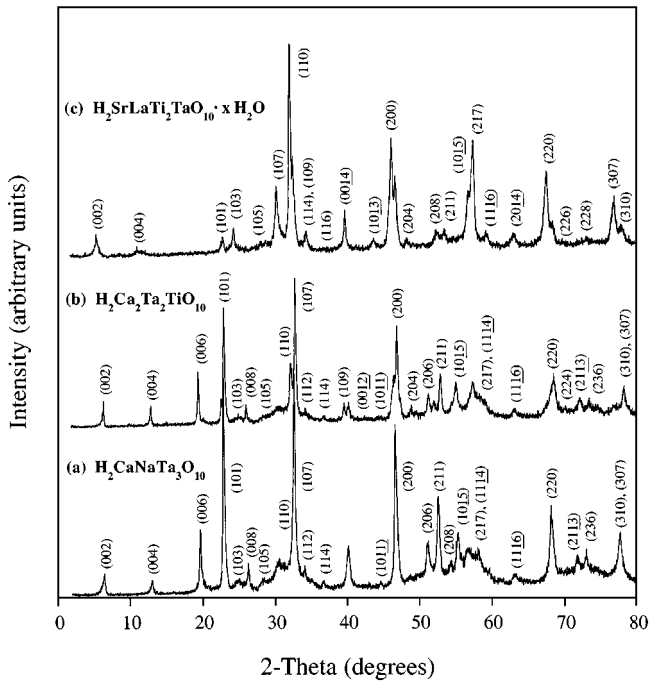

FIG. 3. X-ray powder diffraction patterns of (a) $H_2CaNaTa_3O_{10}$, (b) $H_2Ca_2Ta_2TiO_{10}$, and (c) $H_2SrLaTi_2TaO_{10}\cdot xH_2O$.

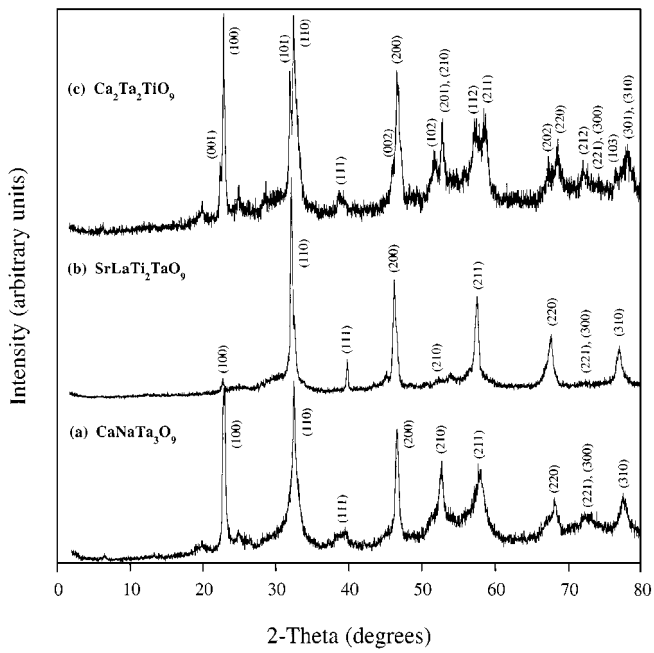

FIG. 5. X-ray powder diffraction patterns of (a) $CaNaTa_3O_9$, (b) $SrLaTi_2TaO_9$, and (c) $Ca_2Ta_2TiO_9$.

and not the lamellar phases) are evidence of low-temperature topochemical dehydration.

Topochemical Dehydration of Ruddlesden–Popper Acids

An interesting feature of many Ruddlesden–Popper acids is that at relatively low temperatures ($< 500^\circ$C), the interlayer protons can be eliminated together with the terminal oxygen atoms of the perovskite block in the topochemical dehydration reaction shown in Fig. 4 (7, 16). Removal of water from the interlayer allows the BO_6 octahedra along the interlayer to collapse, transforming the two-dimensional layered structure into a three-dimensional phase. The resulting cubic phases are inherently *A*-site defective, since only two-thirds of the cations required to fill the *A* sites are contained in the perovskite blocks of the lamellar phases. While many layered perovskites, such as $H_2La_2Ti_3O_{10}$ and $H_2SrTa_2O_7$, topochemically dehydrate and form three-dimensional phases, $H_2Nd_2Ti_3O_{10}$ retains its layered structure upon dehydration to $Nd_2Ti_3O_9$ (31). Our results indicate that all of the solid Ruddlesden–Popper acids presented in this study topochemically dehydrate to form *A*-site deficient three-dimensional perovskites. Additionally, the *A*-site cations disorder into the vacant *A* sites created from the collapse at the interlayer. Similar *A*-site disordering was observed during the topochemical synthesis of $SrTa_{2-x}Nb_xO_6$ (16), $AEu_2Ti_2NbO_9$ (A = Li, Na) (15), and $MEu_2Ti_3O_9$ (M = Ni, Cu, Zn) (15).

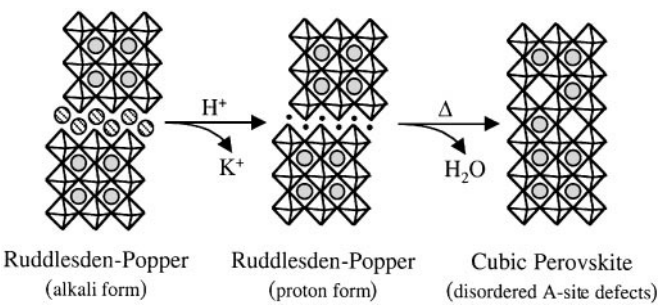

FIG. 4. Schematic representation of the topochemical dehydration of a Ruddlesden–Popper acid to an *A*-site defective cubic perovskite. The octahedra are MO_6 units, and the shaded circles represent the *A*-site and interlayer cations.

$H_2CaNaTa_3O_{10}$ topochemically dehydrates around 500°C to form $CaNaTa_3O_9$, shown in Fig. 5a. The cubic perovskite peaks are broad, indicating some disorder during the topochemical collapse. Peak broadening has been observed previously in similar systems (16) and is likely due to disorder along the *c* axis during the dehydration reaction or random expansion and contraction of the lattice as the *A*-site cations disorder into the vacant *A* sites. A weak low-angle reflection around 6° 2θ is most likely due to regions of unexchanged $K_2CaNaTa_3O_{10}$ that cannot dehydrate. (A structural model based on *A*-site ordering would predict a peak around 7.5° 2θ, as in $AEu_2Ti_3O_9$ (15).) Other unindexed peaks are consistent with small regions of the

crystallites that do not topochemically collapse, as well as the small perovskite impurity present in the original sample. Evidence that topochemical dehydration occurs rather than decomposition to other binary or ternary oxides is provided by the powder diffraction pattern and the lattice parameters. First, no peaks corresponding to other oxide phases could be identified. Second, the lattice parameter for a possible decomposition product $KTaO_3$ is 3.989 Å, while the lattice parameter for $CaNaTa_3O_9$ is only 3.890 Å.

$H_2Ca_2Ta_2TiO_{10}$ and $H_2Sr_2Ta_2TiO_{10}$ also dehydrate to form $Ca_2Ta_2TiO_9$ and $Sr_2Ta_2TiO_9$, respectively. The lattice parameters for the dehydrated phases, shown in Table 1, are similar to the lattice parameters for the *a* axes of the corresponding alkali phases. $H_2SrLaTi_2TaO_{10}$ and $H_2CaLaTi_2TaO_{10}$ topochemically dehydrate to form $SrLaTi_2TaO_9$ and $CaLaTi_2TaO_9$, shown in Fig. 5b. The lattice parameters for $Sr_2Ta_2TiO_9$, $SrLaTi_2TaO_9$, and $CaLaTi_2TaO_9$ are all around 3.91 Å. These values are larger than the lattice parameter of $CaNaTa_3O_9$, which is reasonable considering that the larger Sr^{2+} and La^{3+} cations fill the *A* sites rather than Ca^{2+} and Na^+. This is also consistent with the size variation in the ABO_3 perovskites $CaTiO_3/SrTiO_3$ and $NaTaO_3/KTaO_3$ where the size of the *A*-site cation significantly affects the size of the unit cell (for perovskites having the same *B*-site cations). Likewise, the smaller Ca^{2+} cation in the *A* site of $CaTiO_3$ results in orthorhombic symmetry, just as $Ca_2Ta_2TiO_9$, shown in Fig. 5c, adopts tetragonal symmetry, which is lower symmetry than in the other topochemically synthesized perovskites that have larger *A*-site cations.

CONCLUSIONS

In this paper, we describe the synthesis of new tantalates and titanotantalates that are $n = 3$ members of the Ruddlesden–Popper series of layered perovskites. By optimizing the heating times and temperatures for each system, new and higher-purity phases can be synthesized. The titanotantalates appear to be more susceptible to hydration than their titanate counterparts, which could indicate a high affinity for intercalation and ion exchange that could result in new metastable phases. The proton-exchanged forms of these tantalates and titanotantalates appear to be more acidic than the layered titanates, and have recently been found to intercalate tetrabutylammonium hydroxide, which leads to delamination of the solid into unilamellar colloidal sheets (32). Subsequent layer-by-layer assembly of these sheets, followed by topochemical dehydration, could lead to interesting new thin film perovskites and rationally designed metastable solids.

ACKNOWLEDGMENTS

This work was supported by National Science Foundation Grant CHE-9529202. This material is based upon work supported under a National Science Foundation Graduate Fellowship. T.E.M. thanks Professor Honig for an inspiring late night tour of the Purdue University skull melter, a place where "real" solid state chemistry is done.

REFERENCES

1. (a) S. N. Ruddlesden and P. Popper, *Acta Crystallogr.* **10,** 538 (1957); *Acta Cystallogr.* **11,** 54 (1958); (b) S. Uma, A. R. Raju, and J. Gopalakrishnan, *J. Mater. Chem.* **3,** 709 (1993).
2. J. G. Bednorz and K. A. Müller, *Z. Phys. B* **64,** 189 (1986).
3. T. Kimura, Y. Tomioka, H. Kuwahara, A. Asamitsu, M. Tamura, and Y. Tokura, *Science* **274,** 1698 (1996).
4. (a) M. Dion, M. Ganne, and M. Tournoux, *Mater. Res. Bull.* **16,** 1429 (1981); (b) A. J. Jacobson, J. W. Johnson, and J. T. Lewandowski, *Inorg. Chem.* **24,** 3727 (1985); (c) M. M. J. Treacy, S. B. Rice, A. J. Jacobson, and J. T. Lewandowski, *Chem. Mater.* **2,** 279 (1990).
5. S. Byeon, J. Yoon, and S. Lee, *J. Solid State Chem.* **127,** 119 (1996).
6. J. Gopalakrishnan, S. Uma, and V. Bhat, *Chem. Mater.* **5,** 132 (1993).
7. J. Gopalakrishnan and V. Bhat, *Inorg. Chem.* **26,** 4299 (1987).
8. S. Uma, A. R. Raju, and J. Gopalakrishnan, *J. Mater. Chem.* **3,** 709 (1993).
9. (a) K. Toda, J. Watanabe, and M. Sato, *Solid State Ionics* **90,** 15 (1996); (b) M. Sato, J. Abo, and T. Jin, *Solid State Ionics* **57,** 285 (1992).
10. (a) K. Hyeon and S. Byeon, *Chem. Mater.* **11,** 352 (1999); (b) R. A. McIntyre, A. U. Falster, S. Li, W. B. Simmons, Jr., C. J. O'Connor, and J. B. Wiley, *J. Am. Chem. Soc.* **120,** 217 (1998); (c) J. N. Lalena, B. L. Cushing, A. U. Falster, W. B. Simmons, Jr., C. T. Seip, E. E. Carpenter, C. J. O'Connor, and J. B. Wiley, *Inorg. Chem.* **37,** 4484 (1998); (d) C. H. Mahler, B. L. Cushing, J. N. Lalena, and J. B. Wiley, *Mater. Res. Bull.* **33,** 1581 (1998); (e) B. L. Cushing and J. B. Wiley, *Mater. Res. Bull.* **34,** 271 (1999).
11. M. Fang, C. H. Kim, and T. E. Mallouk, *Chem. Mater.* **11,** 1519 (1999).
12. M. Machida, J. Yabunaka, and T. Kijima, *Chem. Mater.* **12,** 812 (2000).
13. H. Fukuoka, T. Isami, and S. Yamanaka, *Chem. Lett.* 704 (1997).
14. (a) C. N. R. Rao and J. Gopalakrishnan, *in* "New Directions in Solid State Chemistry," 2nd ed., Cambridge Univ. Press, Cambridge, 1997; (b) A. Stein, S. W. Keller, and T. E. Mallouk, *Science* **259,** 1558 (1993); (c) J. Gopalakrishnan, *Chem. Mater.* **7,** 1265 (1995).
15. R. E. Schaak and T. E. Mallouk, *J. Am. Chem. Soc.* **122,** 2798 (2000).
16. P. J. Ollivier and T.E. Mallouk, *Chem. Mater.* **10,** 2585 (1998).
17. V. Thangadurai, G. N. Subbanna, and J. Gopalakrishnan, *Chem. Commun.* 1300 (1998).
18. J. Gopalakrishnan, T. Sivakumar, V. Thangadurai, and G. N. Subbanna, *J. Am. Chem. Soc.* **122,** 6237 (2000).
19. T. A. Kodenkandath, J. N. Lalena, W. L. Zhou, E. E. Carpenter, C. Sangregorio, A. U. Falster, W. B. Simons Jr., C. J. O'Connor, and J. B. Wiley, *J. Am. Chem. Soc.* **121,** 10,743 (1999).
20. T. A. Kodenkandath and J. B. Wiley, *Mat. Res. Bull.*, in press.
21. (a) H. M. Rietveld, *J. Appl. Crystallogr.* **2,** 65 (1969); (b) A. C. Larson, and R. B. von Dreele, "Program Version: PC-98." Los Alamos National Lab. Rep. No. LA-UR-86-748, 1994.
22. K. Toda, Y. Kameo, S. Kurita, and M. Sato, *J. Alloys Compd.* **234,** 19 (1996).
23. N. S. P. Bhuvanesh, M. P. Crosnier-Lopez, H. Duroy, and J. L. Fourquet, *J. Mater. Chem.* **9,** 3093 (1999).
24. M. Toda, M. Takahashi, T. Teranishi, Z. G. Ye, M. Sato, and Y. Hinatsu, *J. Mater. Chem.* **9,** 799 (1999).
25. K. Toda, J. Watanabe, and M. Sato, *Mater. Res. Bull.* **31,** 1427 (1996).

26. N. S. P. Bhuvanesh and J. Gopalakrishnan, *J. Mater. Chem.* **7,** 2297 (1997).
27. K. Toda, T. Taranish, M. Takahashi, Z.Ye, and M. Sato, *Solid State Ionics* **113,** 501 (1998).
28. K. Toda, Y. Kameo, S. Kurita, and M. Sato, *Bull. Chem. Soc. Jpn.* **69,** 349 (1996).
29. M. Sato, J. Abo, and T. Jin, *Solid State Ionics* **57,** 285 (1992).
30. Rietveld analysis yielded the weight fraction of $K_2SrLaTi_2TaO_{10} \cdot xH_2O$ and a perovskite impurity phase, and this weight percent was considered when interpreting the TGA data to obtain the number of waters of hydration per formula unit.
31. M. Richard, L. Brohan, and M. Tournoux, *J. Solid State Chem.* **112,** 345 (1994).
32. R. E. Schaak and T. E. Mallouk, *Chem. Mater.*, in press.